12TH INTERNATIONAL SYMPOSIUM ON FLOW VISUALIZATION
September 10-14, 2006, German Aerospace Center (DLR), Göttingen, Germany

VISUALIZATION OF BUBBLY PROPELLER FLOW WITH DEFOCUSING DIGITAL PARTICLE IMAGE VELOCIMETRY

Emilio Castaño Graff*, Francisco Pereira, Mory Gharib***
***Caltech, Pasadena, California 91125 USA**
****INSEAN, Rome, Italy**

ABSTRACT

A two-blade model ship propeller approximately 66 mm in diameter was driven at about 15 Hz in a circulating water tunnel seeded with bubbles. The flow of the bubbles was imaged with the latest-generation Defocusing Digital Particle Image Velocimetry (DDPIV) camera, yielding all three components of velocity of bubbles as well as population statistics inside a volume approximately 1.5 diameters deep by 2.5 diameters wide in a phase-resolved fashion. Concatenation of phase-locked pairs yields one data point (velocity and population information) every 1 mm in each direction (~1 million data points per phase station), easily resolving the tip vortex and its evolution and entrainment of bubbles. This experiment is exemplary of the capabilities of DDPIV as a flow diagnostic tool

1 INTRODUCTION

Over the past 30 years, particle image velocimetry has evolved into a widely accepted flow diagnostic tool. The advent of commercially available digital imagers simplified the acquisition method (Cho 1989, Willert and Gharib 1991) and the analysis methods evolved accordingly (Keane and Adrian 1992, Westerweel 1997).

Stereo DPIV allowed the third component of velocity to be extracted from two views of a planar domain (Gauthier and Riethmuller 1988), and evolved into the now frequently used Scheimpflug arrangement (Prasad and Jensen 1995). To extract the depth derivative the technique has been extended to multiple planes (Kähler and Kompenhans 2000). However, it remains a planar technique and thus the spatial derivatives are difficult to estimate without complex optical setups. The complexity of the optical train in holographic techniques has made this volumetric technique somewhat undesirable.

Defocusing Digital Particle Image Velocimetry combines the simplicity of DPIV with the desirability of the volumetric measurement domain. The method reconstructs three-dimensional point clouds from digital images and thus it has the added advantage of being able to track marked surfaces and perform particle sizing (the sizing is absolute with an in-situ calibration). The simplicity of DPIV is maintained in that the imaging unit is one-piece and in normal conditions requires only calibration at the time of manufacture and in extreme circumstances. The light source need only illuminate the seed particles in the appropriate volume and thus its alignment to the camera is much less sensitive than in the planar techniques.

2 THE DEFOCUSING CONCEPT AND BASIC THEORY

A point in space off-axis from an aperture will have an image that experiences a lateral offset as the point moves along the axis of the optical system. The defocusing technique embraces this phenomenon and images each point in space through multiple apertures. With knowledge of the basic optical parameters of the system, the relative shift between images can be used to calculate the out-of-plane position of each point. Each defocused particle in space will generate multiple images that form a pattern corresponding to the shape of the aperture layout, but at varying scales (dependent on the distance from the point to the reference plane). In processing the images, it is then necessary to look at all the particle images and find the corresponding images that together complete the aperture layout pattern. Although only two apertures are required to extrapolate the three-dimensional position of a point, in practice at least three apertures are necessary to decrease the number of mismatched particle images ("ghost" particles). Each subsequent aperture added ever decreasingly reducing the position error and the number of ghost particles.

The term "defocusing" in this case is not associated with the blur inherent in the image of a point not on the focal plane of the system. DDPIV does not rely on the image blur to extrapolate the spatial position of a point source, and the entire concept can be explained using pin-hole optics arguments (which imply an infinite depth of field). In practice, the image blur plays a role in the estimation of the sub-pixel location of the particle images. Using separate sensors for each aperture allows for an increase in the aperture separation (without the prohibitive cost of enormous lenses) and for particle image separation so that the particle image matching becomes less ambiguous. Another advantage of separating the aperture spaces is that the seeding density can be much higher than if all apertures formed images on the same sensor.

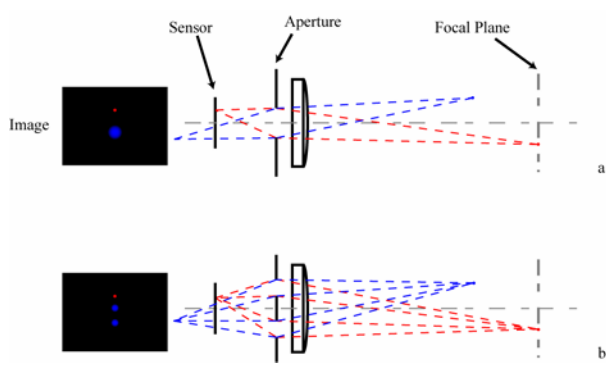

Fig. 1 - A schematic of the defocusing concept. Figure *a* depicts a standard, single-aperture optical system imaging a particle on the focal plane and one ahead of it. The particle not on the focal plane appears as a blurred dot. Figure *b* depicts an optical system with two off-axis apertures, through which the out-of-focus point forms two blurred images. The distance between them is directly related to the characteristics of the optical system (focal length, aperture separation, and distance to the focal plane) and the spatial position of the point source.

The theory behind the imaging system for DDPIV is covered intensively in Pereira and Gharib 2002. Here we present a slightly more generalized form and equate it with the previous work.

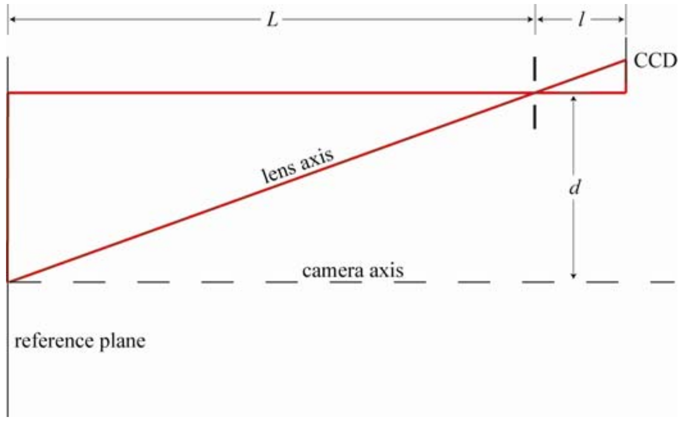

Fig. 2 - A schematic of sensor alignment with respect to the DDPIV camera axis and reference plane.

The arrangement of the multiple sensor/lens systems in a DDPIV camera is such that, at the reference plane, all sensors have an exactly equal field of view, and all apertures are coplanar. This condition is shown in figure 2 for one sensor with the optics replaced by a single aperture. The position of the aperture relative to the DDPIV optical axis (c, d) is a design parameter as is the value of L, the distance from the aperture plane to the reference plane.

Knowing the focal length of the lens f the distance l is calculated by the thin lens equation:

$$\frac{1}{L}+\frac{1}{l}=\frac{1}{f}\Rightarrow l=\frac{Lf}{L-f} \tag{1}$$

With the origin at the intersection of the DDPIV optical axis and the aperture plane, using pinhole optics arguments specify that the position of the center of the sensor in space has coordinates

$$X_C=c\left(1+\frac{f}{L-f}\right),\quad Y_C=d\left(1+\frac{f}{L-f}\right),\quad Z_C=-\frac{fL}{L-f} \tag{2}$$

where c and d are the coordinates of the corresponding aperture relative to the system single optical axis. If the sensor is perfectly aligned (it has center with coordinates as defined by equation 2 and is parallel to the aperture plane) then it can be shown that a point in space with coordinates (X_P, Y_P, Z_P) has image coordinates

$$x=\frac{f}{L-f}\frac{c(L-Z_P)-LX_P}{Z_P},\quad y=\frac{f}{L-f}\frac{d(L-Z_P)-LY_P}{Z_P} \tag{3}$$

Given two apertures i and j, the separation between the particle images is

$$b_{ij}=M\frac{L-Z_P}{Z_p}s_{ij} \tag{4}$$

Here, M is the optical magnification as defined by pinhole optics and s is the separation between apertures i and j. Equation 4 represents mathematically the statement above that each point in space will be imaged as a pattern with the same shape as the aperture layout but at a scale corresponding to the depth of the point in space. It is important to note that the separation is not a function of X_P or Y_P, thus relaxing constraints that would otherwise limit the particle search to a single surface in depth.

To maintain consistency with Pereira and Gharib 2002, we introduce the quantity K:

$$K = \frac{1}{Ms_{ij}L} \tag{5}$$

Now, we can rewrite the image separation (4) in the same form:

$$b_{ij} = \frac{1}{K}\left(\frac{1}{Z_P} - \frac{1}{L}\right) \tag{6}$$

Continuing from (4), the sensitivity of an aperture pair in Z is

$$\frac{\partial b_{ij}}{\partial Z_P} = -\frac{M}{Z_P^2} s_{ij} \tag{7}$$

The coordinates of the point in space can be calculated from its images from (4):

$$Z_P = \frac{L}{1 + \frac{b_{ij}}{M}\frac{1}{s_{ij}}} \tag{8}$$

Knowing the Z coordinate of the point, the X and Y coordinates are the coordinates of the centroid of the image pattern, and can be written as:

$$X_P = \bar{c}\left(1 - \frac{Z_P}{L}\right) - \bar{x}M\frac{Z_P}{L}, \quad Y_P = \bar{d}\left(1 - \frac{Z_P}{L}\right) - \bar{y}M\frac{Z_P}{L} \tag{9}$$

where ($\bar{c}$, $\bar{d}$) are the coordinates of the matched pattern centroid.

3 DDPIV SYSTEMS IN PRACTICE

Even though the theory suggests that only two apertures are necessary, normally this is insufficient. The only robust way to match particle images together is the aperture layout pattern and thus having only two apertures leads to a likely chance of mismatch in dense fields. In practice DDPIV systems use three apertures arranged in an equilateral triangle. This arrangement guarantees that the sensitivity between any two apertures is equal. There are cases where this advantage can be sacrificed in favor of package size, as was done in the underwater system for full-scale field experiments on naval vessels. Sensors are typically double-exposure interline transfer CCD's as in many other PIV applications.

Fig. 3 - An underwater DDPIV system with a shortened aperture layout to reduce drag.

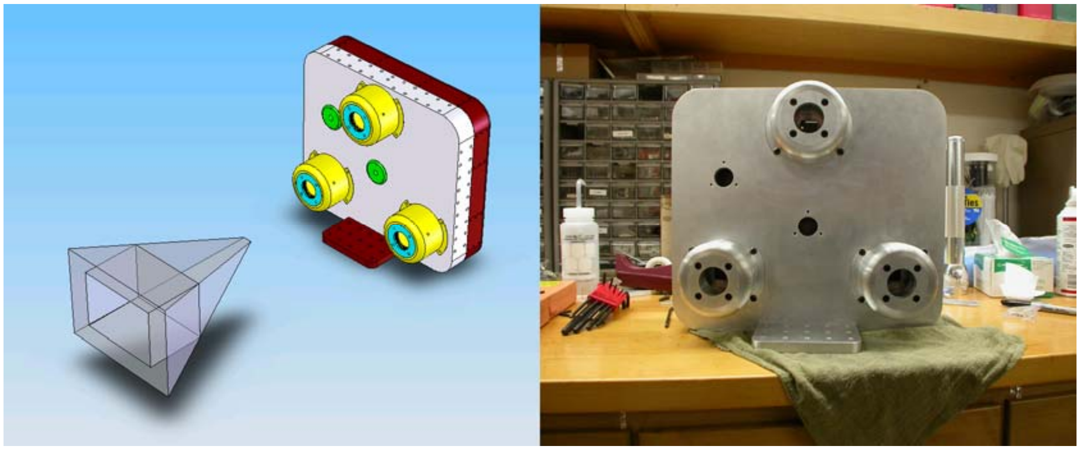

Fig. 4 - The latest-generation DDPIV camera use to obtain the results presented here. The CAD model shows a geometrical estimate of the measurement domain (the asymmetric pyramid). The "characteristic volume" – the number used to describe the measurement domain – is the side length of the largest rectangular prism inscribable within this pyramid-like shape.

Due to manufacturing tolerances and other factors (real optics vs. pinholes), it is impossible for real systems to meet the conditions established in section 2. All real cameras require an initial calibration to correct for errors in the placement of the sensors and aberrations as well as differences in the lenses.

This calibration, or "multiplane dewarping", need only be performed at the time of assembly. The underwater system show in figure 3, for example, was calibrated once in-lab, then mounted to the transom of the R/V Athena for 3 12-hour trips to the Gulf of Mexico. Once it returned to the lab, it showed no loss in precision in the mapping of particle fields.

Multiplane dewarping consists of imaging several known grid planes throughout the volume. It is similar to calibrations commonly used for SPIV systems but differs in how the correction is applied to experimental data.

A target displaying a grid of dots with a calibrated spacing is translated across the desirable measurement volume along the depth-axis in a discretionary number of steps. At each Z-station, the target is imaged through the DDPIV camera. The system's mechanical and optical imperfections, (e.g. sensor misalignment, lens aberrations, flow setup such as windows and fluid media optical properties) are recorded as a distortion of the perfect calibration grid. The distorted dot coordinates are measured using sub-pixel techniques and are then associated to the perfect grid coordinates. A multi-parameter non-linear optimization is then performed to derive a family of best mapping functions, in the least-mean squares sense, between the distorted grid and the ideal grid. The process provides 2nd, 3rd and 4th order polynomial-type functions. A family of these functions is calculated independently for each calibration Z-station.

Experimental data is corrected using these calibration coefficients, but whereas most dewarping techniques apply to the images themselves, in the defocusing method the correction is applied to the particle image coordinates in two distinct stages. In a first stage, a coarse pattern matching is performed on the complete dataset using the calibration data obtained at one given plane (usually the reference plane), i.e. the particle image coordinates are corrected (or "dewarped") using one single mapping function. This coarse analysis provides a means to calculate a rough estimate of every single particle location in space, which is used to select the two nearest calibration stations for the second stage. The corresponding mapping functions are applied to the distorted particle image coordinates and a second and final pattern matching is performed using tighter tolerances. This two-stage process allows for a higher degree of accuracy in the measurement of the depth location Z, and reduces drastically the population of ghost particles.

In an experimental setting, the volume is illuminated by a pulsed light source, be it a laser or a strobe, and then the images are converted to three-dimensional point clouds. One can then apply a particle sizing calibration set to these fields to obtain absolute size, though relative size can be calculated without any additional calibration. Once each frame triplet is converted to a point cloud in space coordinates, the velocity can be calculated either by a three-dimensional cross-correlation (PIV) or, if the seeding density is appropriate, by three-dimensional particle tracking (PTV) (see Pereira et al. 2006).

The resulting three-component volumetric vector fields contain a wealth of information. Spatial derivatives can be calculated in all three directions, thus quantities like vorticity and divergence can be calculated completely. The vorticity can be visualized either by isosurfaces or by "streamlines", which in some sense correspond to vorticity lines. "Virtual dye" visualizations can be performed by computationally placing particles in the vector fields and integrating their paths in time.

4 ACCURACY OF DDPIV

The accuracy of modern defocusing cameras is excellent. Accuracy of reconstructed position in X and Y are on the order of 0.01% and in Z about 3.5 times less accurate (where the % denotes the error in position as a percentage of the volume size). The increases in accuracy with respect to Pereira and Gharib 2002 are attributed to advancements in the design and construction of the cameras both structurally and optically.

Figure 5 shows a close-up of measured particle tracks in a slow-moving flow: a real example of the position reconstruction accuracy of the system. The total volume imaged was about 150x100x100 mm; the section shown here is merely a 2mm square.

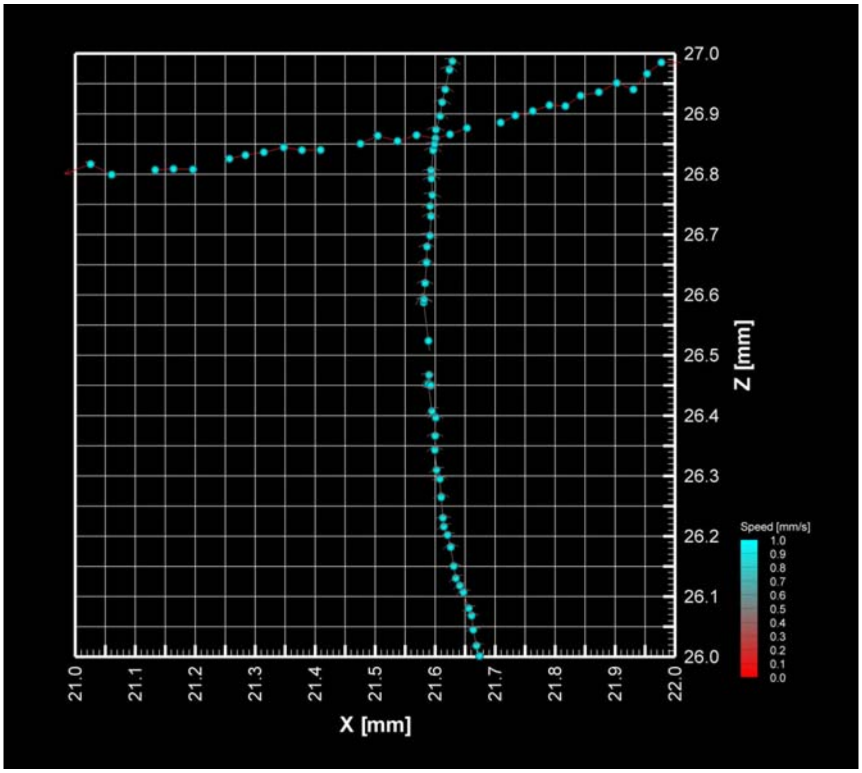

Fig. 5 - Detail of particle tracks measured by the latest-generation camera. The increased error in Z can be seen here as "jitter" in the path of the [primarily] horizontally-moving particle and as uneven spacing in the [primarily] vertically-moving particle.

Details of the accuracy and yield of the particle sizing method and specific particle tracking algorithms can be found in Pereira and Gharib 2004 and Pereira et al. 2006.

5 EXPERIMENTAL SETUP FOR PROPELLER EXPERIMENT

The model ship propeller in this experiment was driven by a stepper motor via a timing belt with the pulley located downstream of the propeller. The stepper motor axle was set up with a photo-interrupter so precise synchronization between the propeller and the laser/camera timing circuit was achieved. For an approximate propeller speed of 15 Hz, 200 pairs each were captured at phase stations 5 degrees apart for 180 degrees of revolution.

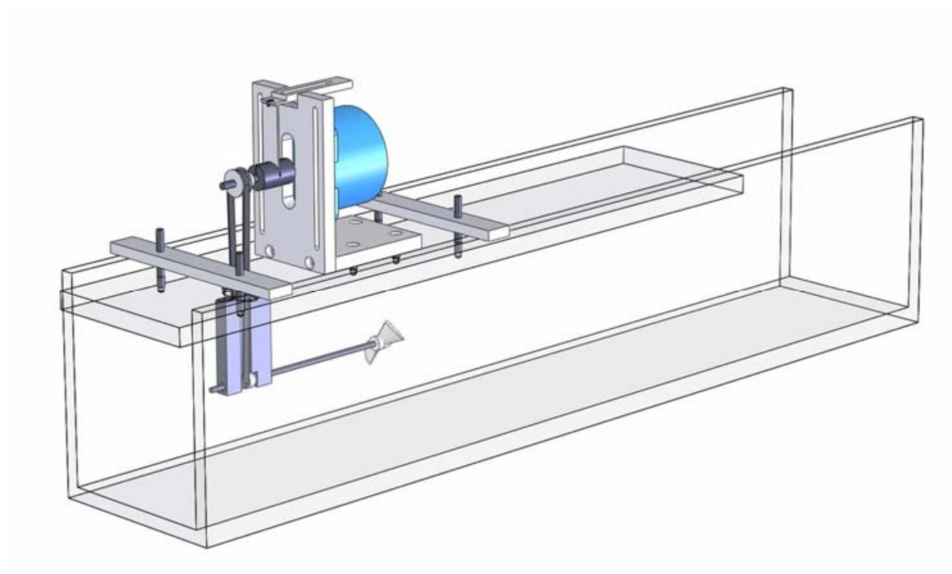

Fig. 6 - CAD model of the propeller setup shown over the tunnel test section.

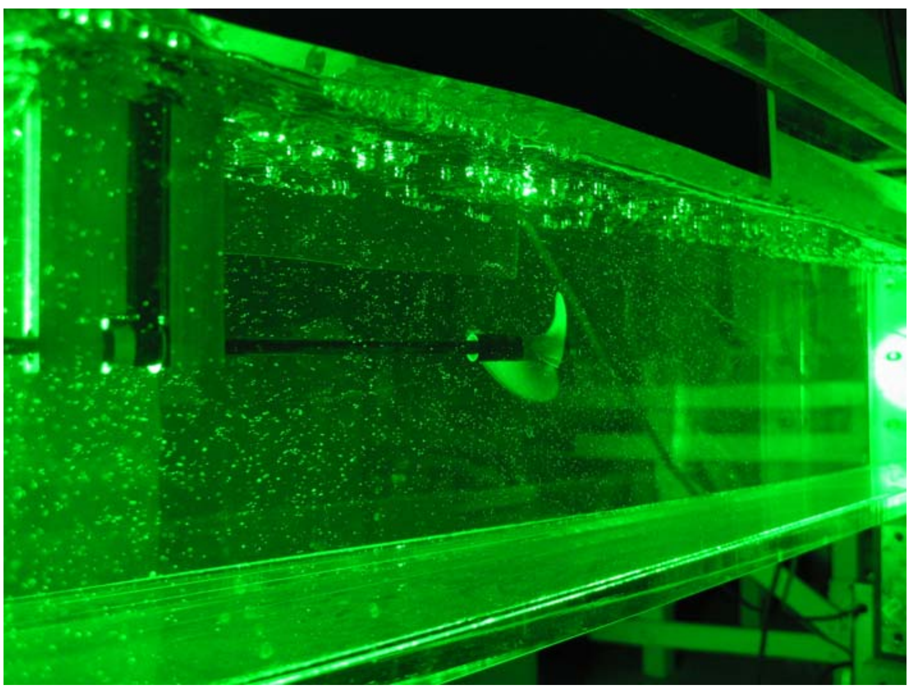

Fig. 7 - Photograph of the propeller in the tunnel during a run.

6 RESULTS

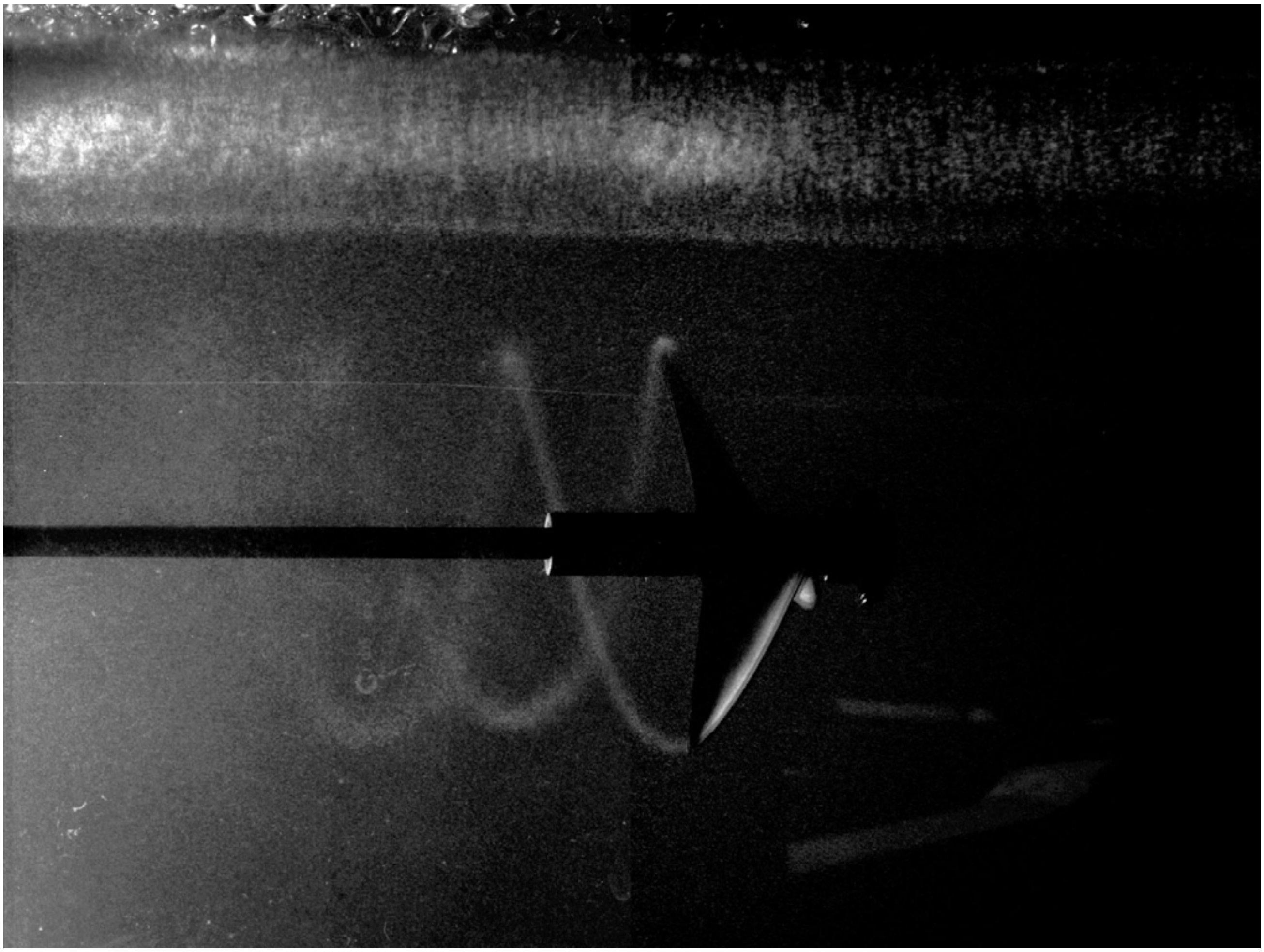

Fig. 8 – Average of 200 images for one phase station for one sensor from the defocusing camera. The concentration of bubbles by the tip vortex is very clear.

Images were preprocessed by masking the reflection of the laser by the propeller blades. Processing of the images yielded on average about 11,000 reconstructed bubble positions per frame; subsequently the tracking algorithm yielded about 7,000 vectors.

The 400 three-dimensional point clouds for each phase station were sorted into a three-dimensional grid of 2mm-cubical elements spaced 1mm apart in each direction yielding for each element the total number of bubbles and the average number of bubbles per frame. Had an in-situ calibration with known particle sizes been performed, the data would also include real calibrated values for average bubble size and void fraction.

The 200 vector fields for each phase station were sorted in a similar manner, yielding an average three-component velocity at each element. The resulting high-resolution ordered grid lends itself well to calculation of derivatives such as vorticity which were not calculated for this experiment due to the seeding being bubbles and not particles.

Figure 9 shows a slice at the axis of the propeller of the resulting vector field for one phase station. This slice is roughly equivalent to a data set acquired with a stereo-DPIV setup, but there are 80 such slices in this Defocusing-DPIV volume. The propeller shown is for representation only, it only roughly equals the real propeller in shape (but very closely in size). The velocity fields presented here are unfiltered (no outlier correction or smoothing).

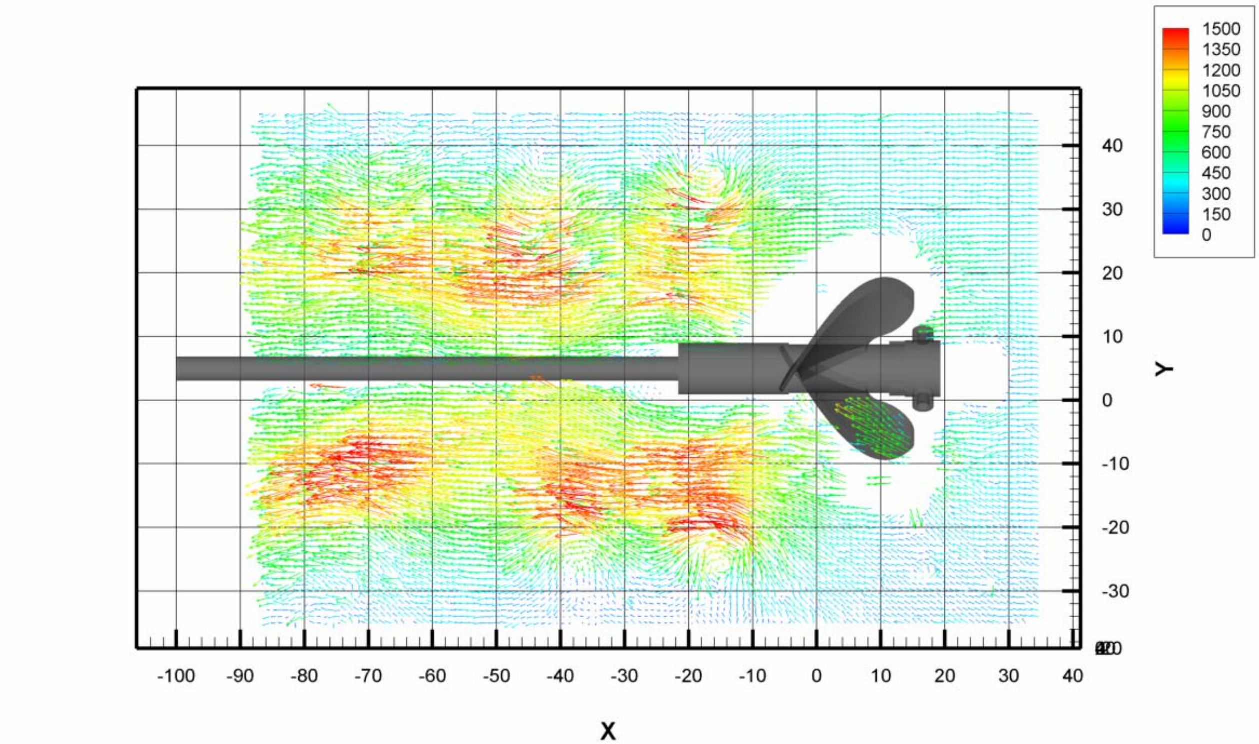

Fig. 9 – One slice of the velocity field for one phase station in the experiment. Units are mm, color code is for velocity (in mm/sec)

For the same data set we can include the bubble population data by forming isosurfaces of average population as shown in the close-up of figure 10. The volume enclosed in the blue region has at least about 3 times the number of bubbles that the free stream has.

Looking at the entire volume in figure 11 (replacing the vectors with instantaneous streamlines)

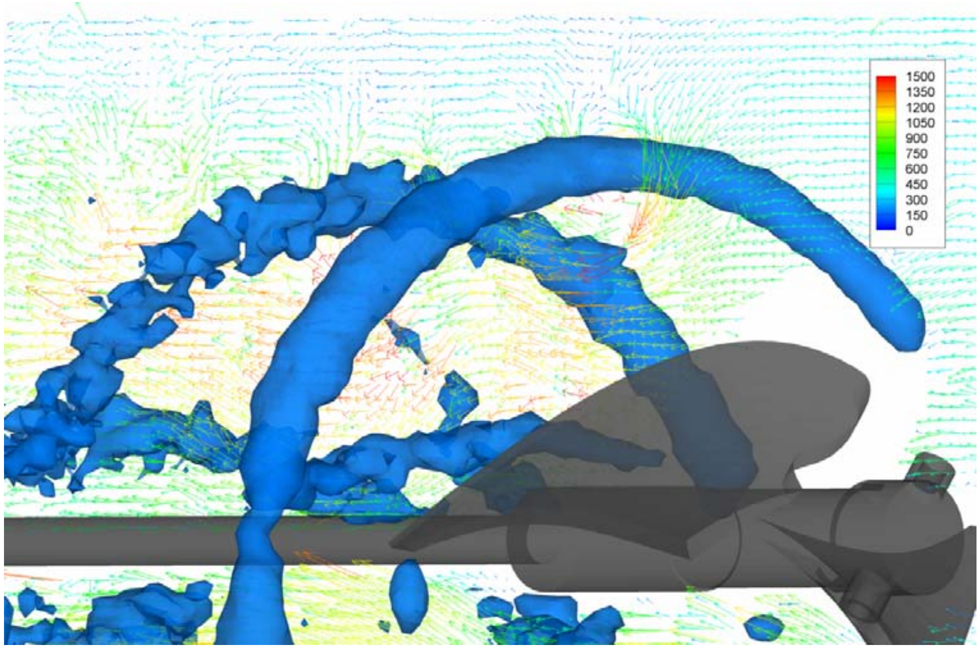

Fig. 10 - Detail of the vortex (depicted as bubble population iso-surface) and velocity field for the same slice as figure 9.

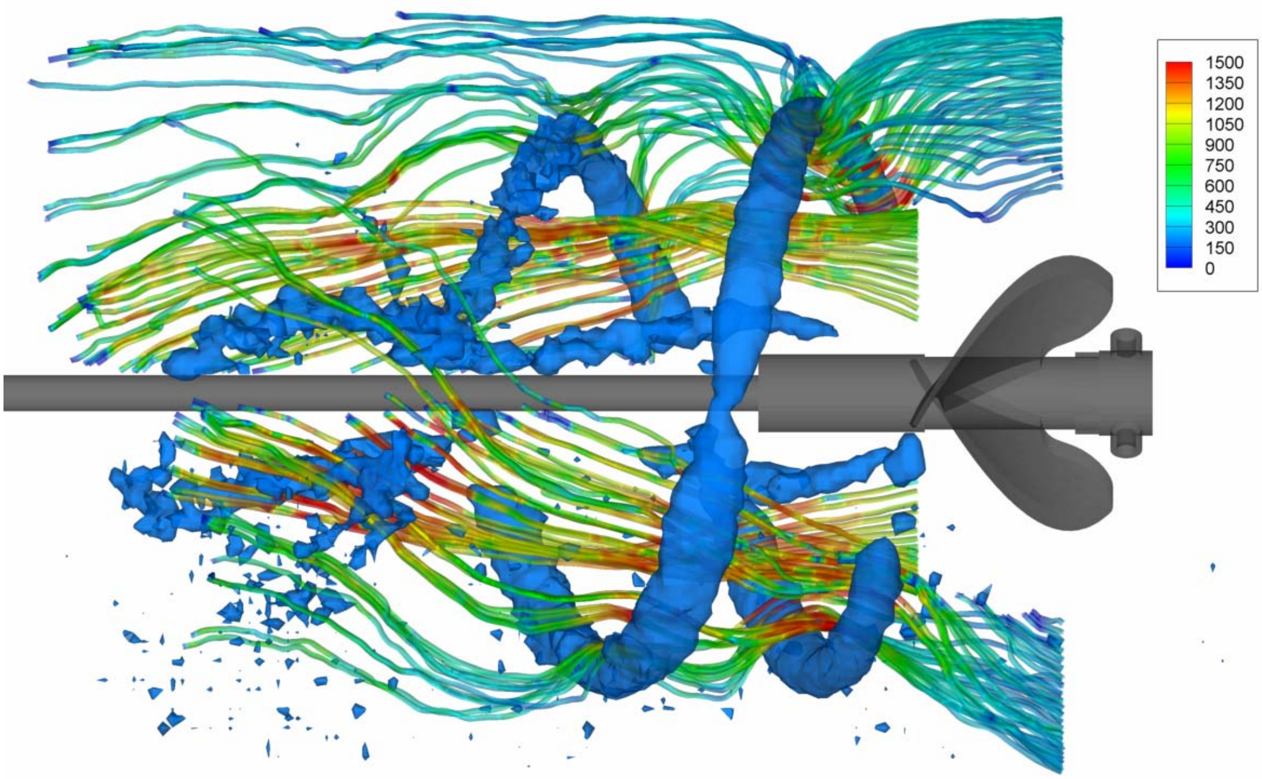

Figure 11 - Full-volume view of the velocity field (represented by two concentric rings of streamlines) and population field (blue blobs).

Note in figure 11 the appearance of a second vortex near the shaft. This vortex is not visible in the average image (figure 8), but is clearly discernable in the population data. It is suspected that this vortex emanates from the set-screws holding the propeller to the shaft.

7 SUMMARY AND ACKNOWLEDGEMENT

Defocusing DPIV is a fully-volumetric, three-component PIV method suitable for the study of flows, sprays, and surface-flow interaction. Its rigid, single-assembly setup makes it suitable for field studies and maximizes the period of time between calibrations. In the limit of a thin sheet, it can also serve as a standard DPIV or alternative stereo-DPIV camera.

Development of DDPIV has been supported by the Office of Naval Research The defocusing technique is protected by US Patent 6,278,847.

REFERENCES

1. Cho Y C. Digital image velocimetry. *Appl. Opt.*, 28, pp 740-8, 1989.
2. Gauthier V, Riethmuller M L. Application of PIDV to complex flows: measurements of the third component. Kármán institute for fluid mechanics – *Particle Image Displacement Velocimetry*. Belgium: Rhode-Saint-Genèse, 1988.
3. Graff E C, Pereira F, Milano M, Gharib M. The capabilities of defocused digital particle image velocimetry. *6th International Symposium on Particle Image Velocimetery*. Pasadena, California, Sept. 21-23 2005.
4. Kähler C J, Kompenhans J. Fundamentals of multiple plane stereo particle image velocimetry. *Exp. Fluids* 29, pp S070-7, 2000.
5. Keane R D, Adrian R J. Theory of cross-correlation analysis of PIV images. *Appl. Sci. Res.*, 49, pp 191-215, 1992.
6. Pereira F, Gharib M. Defocusing digital particle image velocimetry and the three-dimensional characterization of two-phase flows. *Meas. Sci. Technol.*, 13, pp 683-694, 2002.
7. Pereira F, Gharib M. A method for three-dimensional particle sizing in two-phase flows. *Meas. Sci. Technol.*, 15, pp 2029-2038, 2004.
8. Pereira F, Gharib M; Dabiri D; Modarress D. Defocusing digital particle image velocimetry: a 3-component 3-dimensional DPIV measurement technique. Application to bubbly flows. *Exp. Fluids*, 29, pp S78-84, 2000.
9. Pereira F, Stüer H., Graff E C, Gharib M. Two-frame 3D particle tracking. *Meas. Sci. Technol.*, 17, pp 1680-1692, 2006.
10. Prasad A K; Jensen K. Scheimpflug stereocamera for particle image velocimetry in liquid flows. *Appl. Opt.*, 34, pp 7092-9, 1995.
11. Westerweel J. Fundamentals of digital particle image velocimetry. *Meas. Sci. Technol.*, 8, pp 1379-92, 1997.
12. Willert C E, Gharib M. Digital particle image velocimetry. *Exp. Fluids*, 10, pp 181-93, 1991.
13. Willert C E, Gharib M. Three-dimensional particle imaging with a single camera. *Exp. Fluids*, 12, pp 53-358, 1992.